Dendritic Spacing and Macrosegregation Affecting Microhardness of an Al-Si-Mg Alloy Solidified Under Unsteady State Conditions

Cássio da Silva[a], Thiago Soares[b], Noé Cheung[b] , Amauri Garcia[b], Danieli A. P. Reis[a],

*Crystopher Brito[c] * *

[a]*Universidade Federal de São Paulo (UNIFESP), Departamento de Ciência e Tecnologia, 12231-280, São José dos Campos, SP, Brasil*
[b]*Universidade Estadual de Campinas (UNICAMP), Departamento de Engenharia de Manufatura e Materiais, 13083–860, Campinas, SP, Brasil*
[c]*Universidade do Estado de São Paulo (UNESP), 13876-750, São João da Boa Vista, SP, Brasil*

The prediction of microstructure morphology is fundamental for the manufacture of metallic components, since the expected levels of mechanical properties will be associated with the final aspects of the microstructure. In this work, an Al-7wt.%Si-3wt.%Mg alloy was directionally solidified in unsteady state conditions in order to investigate the influence of the addition of 3wt.%Mg to an Al-7wt.%Si alloy on the solidification evolution. The microstructure of the examined alloy is shown to be characterized by a more complex arrangement of phases, as compared to that of the Al-7wt.%Si alloy, which includes the binary (α-Al+Mg_2Si) and refined ternary (α-Al+Si+Mg_2Si+Fe-rich IMC) eutectic mixtures. A higher Vickers hardness profile is shown to be associated with a more refined microstructural arrangement. However, for cooling rates lower than 2K/s the microhardness is shown to increase with the increase in the microstructural spacing, which is shown to occur caused by Si macrosegregation and higher content of free Mg.

Keywords: *Al-Si-Mg alloys, solidification, microstructure, intermetallic compound, microhardness.*

1. Introduction

Al-Si cast alloys have been widely employed in the manufacture of engine components, such as cylinder heads and engine blocks. This class of alloys combines high strength to weight ratio, excellent thermal conductivity, wear and corrosion resistance. All these characteristics and properties make these alloys potential materials to the replacement of cast iron[1,2]. The engine represents on average, about 5% of the entire vehicle mass. One of the biggest challenges of the today's designers is to render high efficiency with low energy consumption and low gas emission. This scenario has been ideal for the development of light alloys, and particularly, the development of aluminum alloys is thus far from being finished. It is known that reducing weight is a very effective way to lower a vehicle´s fuel consumption. Therefore, the reduction of wall thickness without compromising the resistance to the stresses acting inside an engine is one of the main challenges facing aluminum casting industry. The A356 aluminum alloy is an important Al-Si-Mg structural material offering good specific strength associated with high levels of ductility, and excellent wear as well as corrosion resistances. Binary Al-Si alloys do not harden via heat treatment, but the addition of Mg improves the mechanical strength due to the precipitation of the Mg_2Si intermetallics (IMC). This phase is very efficient to increase the mechanical strength at room temperature of 3xx.x and 6xxx series aluminum alloys [3-7].

The use of the Al-7wt.%Si-0.3wt.%Mg alloy has been outstanding in the production of aluminum castings due to its excellent castability and excellent achievement of mechanical properties after heat treatment[4,5]. Although the literature contains several works on the influence of Si and the cooling rate on the microstructure of Al-Si alloys, there is not much information concerning the concomitant influence of the Mg content and the cooling rate on the morphology of as-solidified microstructures[5]. In order to form the Mg_2Si IMC, Mg is usually added to Al-Si alloys in the range 0.3 to 0.6 wt.% [6]. In hypoeutectic alloys, this Mg content gives rise to the formation of Mg_2Si in the form of fine needles in the ternary eutectic mixture (Al + Si + Mg_2Si). The Mg_2Si IMC (or β phase) is a face-centered cubic crystal (FCC), with melting point of 1087°C, specific mass of 1.88g/cm³ and Vickers hardness of 456HV[6]. At room temperature, the microhardness of this IMC can reach 546HV whereas in one hour at 300°C this value drops to 180HV, revealing that the Mg_2Si has low thermal stability. In this case, metastable coherent Mg_2Si phases (β' and β'' phases), which can be achieved by appropriate heat treatments, may be very effective reinforcing phases [6,7].

Recently, some studies have analyzed the effect of Mg contents above 3wt.% on the microstructure of Al-Si based alloys. According to Mandal and Makhlouf [8], the addition of Mg (in the range from 1 to 5 wt.%) in hypereutectic Al-14wt.%Si-0.2wt.%Fe alloys induce the formation of a

*e-mail: crystopher.brito@unesp.br

eutectic mixture of Si and Mg_2Si particles surrounding the α-Al dendritic matrix. Tebib et al. [4] reported that an Al-15wt.%Si-14wt.%Mg-4wt.%Cu hypereutectic alloy can be considered a metal/matrix compound, where the primary phase Mg_2Si (in the form of dendrites) acts as a homogeneously distributed hard reinforcement in a strong and ductile eutectic matrix (Al + Si + Mg_2Si). In this microstructural pattern, the Mg_2Si IMC would reinforce the matrix during its plastic deformation[4]. On the other hand, the literature is scarce on studies concerning the effect of Mg contents above 1wt.% on Al-Si-Mg hypoeutectic alloys.

Alloying elements such as Mg, Cu, Zn, Ni, Cr, Pb, Sn, Mn and Fe are generally added to Al–Si alloys in order to achieve mechanical properties and corrosion resistance for specific applications. However, care should be taken with the alloy Fe content, due to detrimental effects to mechanical and corrosion resistances caused by the formation of IMCs, such as the needle-like β-Al_5FeSi [6,9-12].

Iron has low solubility in Aluminum[6], so Fe contents higher than 0.03wt.% led to the formation of Fe-rich IMCs, whose morphologies depend on the solidification cooling rate and the chemical composition of the alloy[13]. Basically, three patterns have been reported in the literature: acicular, Chinese script, and fishbone-like (or skeleton-like shape). The β-AlSiFe phase (Al_5SiFe), due to its hard and brittle characteristics, is considered the most harmful for Al alloys. When Mg is present in Al-Si alloys containing Fe, the π-AlSiFeMg phase ($Al_8Mg_3FeSi_6$) is formed, which is also deleterious to the mechanical properties, responsible for reducing the ductility of Al-Si alloys[4]. In general, raw material is increasingly scarce due to the global consumption of limited resources. Currently, aluminum is the second most used metal in human activities. Due to the high cost production of primary aluminum, and due to the finite reserves of bauxite (main aluminum ore), the recycling of this metal is fundamental with a view to providing a growing share of total aluminum supply[14]. Efforts have been made to guarantee the quality of recycled aluminum in order to comply with the designed properties. Therefore, it is important to understand how the Fe content will influence the formation of IMCs in Al-Si-Mg castings, for determining the tolerances of Fe content in Al alloys when recycled aluminum is employed [4,15,16].

Peres et al.[17] analyzed the microstructural morphology of Al-Si hypoeutectic alloys produced by a directional solidification technique. The authors observed for a wide range of solidification cooling rates, a microstructure composed essentially of a dendritic α-Al matrix with a eutectic mixture, formed by Al + Si, with Si in the shape of needles, located in the interdendritic regions. Canté et al.[14] evaluated the effects of the cooling rate (in the range of 0.5 to 28K/s) and of the Fe content on the microstructure of an Al-9wt%Si alloy. Coarsening of secondary ($λ_2$) and tertiary ($λ_3$) dendritic arms was observed to occur with decreasing cooling rates, as well as with decreasing incidence of acicular β- AlSiFe IMC (also

associated with the decrease in cooling rate). The β- AlSiFe IMC particles are distributed between the dendritic arms, $λ_2$ and $λ_3$, becoming coarser with the reduction in cooling rate. The coarsest microstructure was shown to be associated with the lowest ultimate tensile strength, and to a substantial 50% reduction in the elongation-to-fracture of this alloy.

Brito et al.[18] reported that the morphology of the Al-rich matrix of an Al-3wt.%Mg-1wt.% Si alloy changes from cellular to dendritic for solidification cooling rates less than 1 K/s, and that a mixture of Mg_2Si and β-AlFeSi IMCs were shown to be distributed in the intercellular and interdendritic regions as eutectic compounds. It was shown that the Vickers microhardness (HV) exhibited an increasing trend with the decrease in the cell spacing ($λ_C$), however, an inverse behavior with respect to the primary dendritic arm spacing, $λ_1$, was observed, where HV increased with the coarsening of $λ_1$. The authors attributed the latter behavior to the better distribution of IMCs throughout the interdendritic regions. In a recent work, Brito et al.[18] have observed that a more refined microstructural arrangement (both matrix and IMCs) showed better corrosion resistance in a 0.06M NaCl solution. The mechanical properties showed similar behavior, and the best combination between ultimate tensile strength and elongation-to-fracture was obtained for the most refined cellular microstructural arrangement [19].

The literature is still scarce of researches on the effects of solidification thermal parameters, macrosegregation, and the scale of microstructure dendritic arrays on the mechanical properties of hypoeutectic Al-Si alloys castings with Mg contents higher than 1wt.%. In order to obtain a directionally solidified (DS) casting under unsteady-state solidification conditions, a water-cooled solidification setup was used, which permitted a wide range of cooling rates to be investigated. The objective of the present work is to analyze the influence of the addition of 3wt.%Mg to an Al-7wt.%Si alloy on the dendritic growth of the Al-rich matrix, and to establish correlations between the dendritic scale of the microstructure, nature and fractions of precipitated IMCs, and the resulting microhardness along the length of the DS casting.

2. Materials and Methods

The Al-7wt.%Si-3wt.%Mg alloy was prepared from commercially pure Al, Si and Mg-Al master alloy. The alloy was directionally solidified in a solidification apparatus, in which heat was removed from a water-cooled bottom, promoting vertical upward unsteady-state solidification. Details concerning the solidification apparatus can be found in a previous study[20] and in Figure 1(a). When a melt temperature of about 35°C above the alloy *liquidus* temperature (T_L) was achieved, the heating system was switched off and at the same time the cooling system was activated, allowing the start of solidification. With a view

Dendritic Spacing and Macrosegregation Affecting Microhardness of an Al-Si-Mg Alloy Solidified Under
Unsteady State Conditions

3

to determining the cooling rate during solidification, eight (8) fine type K thermocouples (0.2 mm diameter wire) were placed in the geometrical center of the cylindrical mold cavity along its length. Figure 1(b) shows the Al-7%wt.Si-xMg pseudo binary phase diagram, calculated by the Thermo-Calc software, where a vertical dashed line indicates the nominal composition of the examined alloy.

The microstructural analysis was carried out on cross and longitudinal sections of samples extracted from the DS casting at the positions: 5, 10, 15, 20, 25, 30, 40, 50, 60, 70, 80, 90 and 100mm from the water-cooled bottom. Subsequently, the samples were ground with sandpapers, and polished with 1μm diamond paste. No chemical etching was required to reveal the microstructure. Optical microscopy was performed using an Olympus Inverted Metallurgical Microscope (model 41GX). The primary (λ_1), secondary (λ_2) and tertiary dendritic arm spacings (λ_3) were measured from optical images referring to the aforementioned sections along the length of the alloy casting. The triangle method[21] was used in order to perform the measurements of λ_1 at the cross sections. The intercept method[20] was adopted for measuring λ_2 and λ_3 at the longitudinal sections. At least 30 measurements were performed for each selected position along the length of the casting. The IMCs were characterized by SEM micrographs and microanalysis using a ZEISS Scanning Electron Microscope (ZEISS-EVO-MA15), equipped with an Energy Dispersive Spectrometer (EDS) model OXFORD X-MAX.

A detailed analysis of area fractions (AF) of the IMC particles have been determined for each sample associated with different positions along the length of the DS casting. Dimensionless shape factors (circularity-C and aspect ratio-AR) of the IMC particles were defined by a relation between the area of the particle surface (S) and its perimeter ($C = 4\pi S/p^2$) for circularity [14, 21]. The circularity factor varies from 1.0 for a perfect circle, decreasing up to zero with the increasing complexity of the morphology of the examined particles.

X-Ray Fluorescence (XRF) analyses were carried out on cross-section samples, using a Rigaku device, model RIX3100, target area of 100mm². The patterns of X-ray Diffraction (XRD) analyses were obtained by a XRD diffractometer X'Pert Pro model MRD XL with a 2-theta range from 35 to 90 deg, Cu-Kα radiation with a wavelength of 0.15406 Å. Vickers microhardness tests were performed in a Shimadzu HRV-2 microdurometer according to the ASTM E384 standard [22]. Twenty indentations were performed for each sample. A 0.5 kgf load and a dwell time of 15 seconds of loading were used.

3. Results and Discussion

Figure 2(a) shows the macrostructure of the DS Al-7wt.%Si-3wt.%Mg alloy casting. The macrostructure morphology was characterized by columnar grains from bottom to the top of the casting allowing quantitative microstructural analyses of primary, secondary and tertiary dendritic arm spacings.
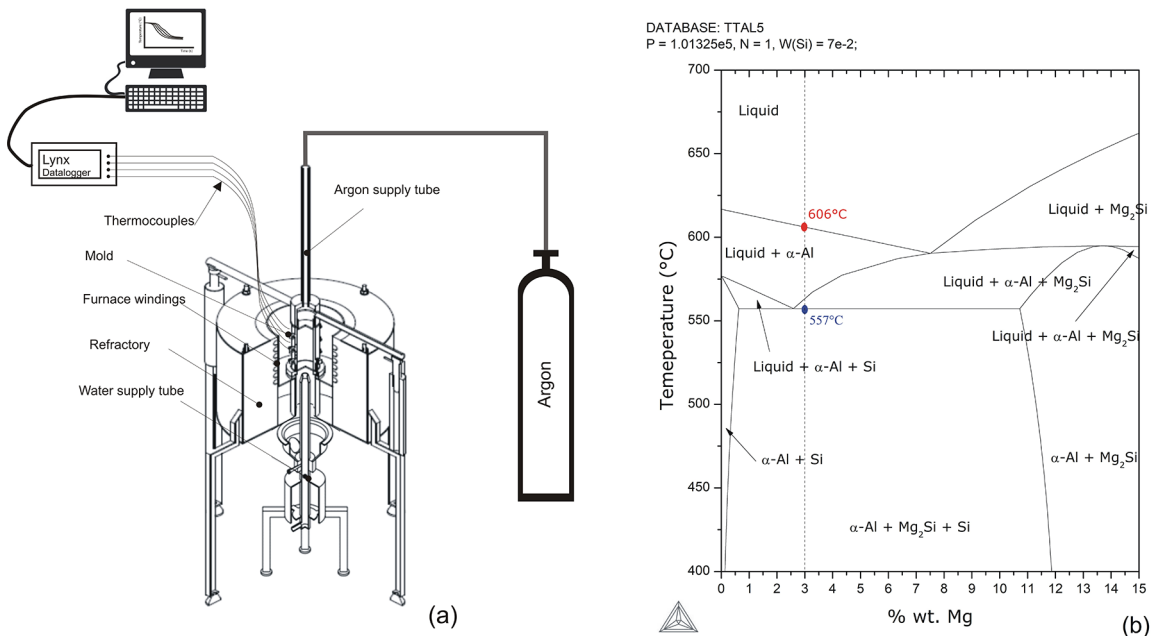

Figure 1. a) Schematic representation of the water-cooled upward directional solidification system; **b)** Pseudo binary phase diagram calculated by the Thermo-Calc software (database TTAL5). The vertical dashed line indicates the examined alloy composition.
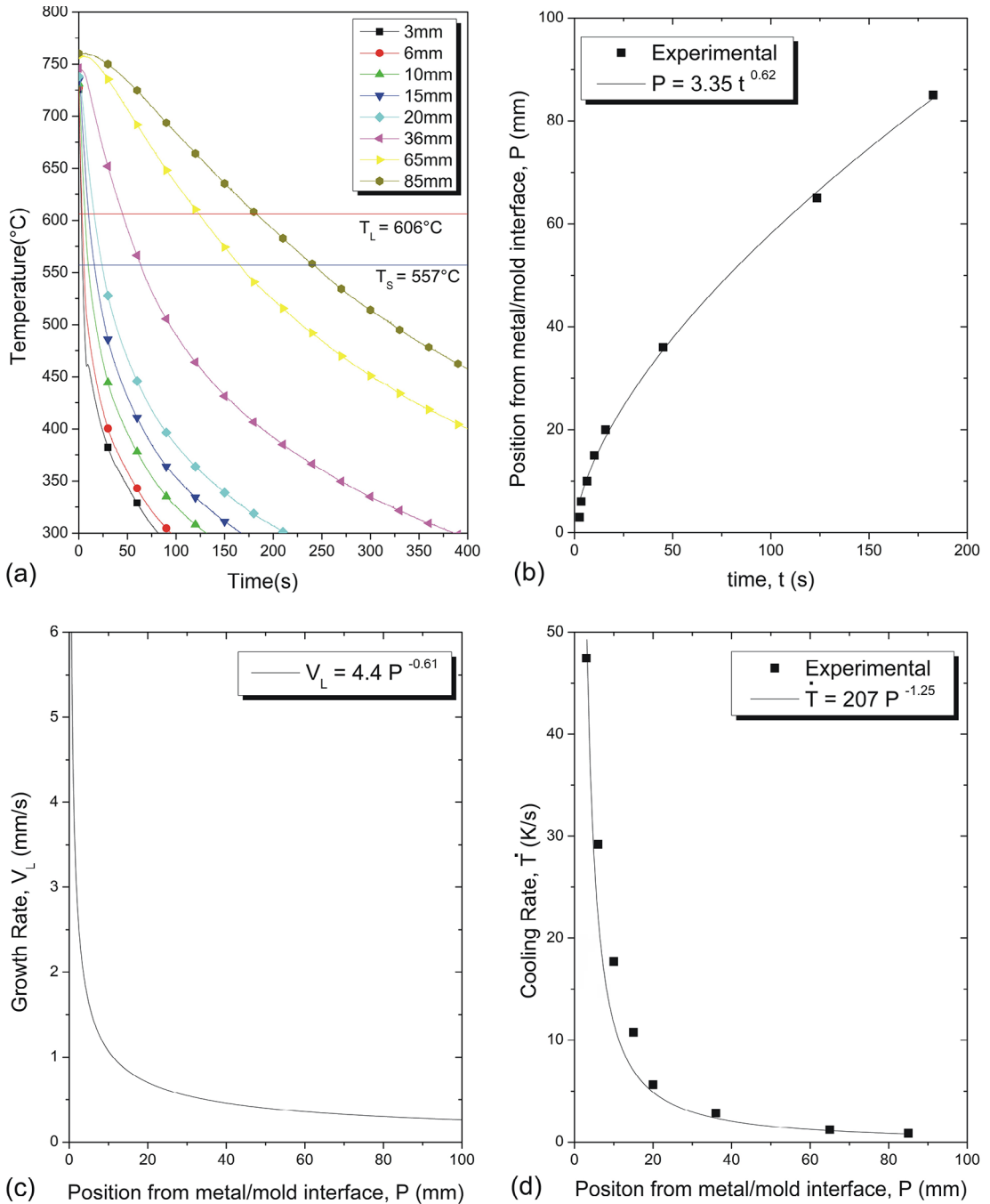
Figure 2(b) shows Si, Mg and Fe contents along the entire DS casting length, obtained by X-ray Fluorescence (XRF). The solute partition coefficient (k_0) of all alloying elements is less than unity ($k_0 < 1$), which promotes the rejection of the solutes ahead of the solid/liquid interface. A negative segregation of Si, ranging from ~ 6wt.% (on the base) to ~ 8.5wt.% (at top of DS casting) was observed. Similar Si segregation behavior was reported for Al-Si-Sn [11] and Al-Si-Cu[23] alloys solidified in the same DS apparatus. The Mg profile was fairly constant along the entire DS casting length, and no significant segregation of this element occurred. The density of Mg (ρ_{Mg}) is lower than that of Al (ρ_{Al}); that is: ρ_{Mg} ~ 70% ρ_{Al} [24]. Due to this fact, increase in the Mg content ahead the solidification interface was expected to occur. However, this did not occur, as shown in Figure 2b. Brito et al.[17] have observed a similar behavior when analyzing compositions of samples extracted along the length of a DS Al-3wt.%Mg-1wt.%Si alloy casting. Vreeman and Incropera [25] have reported positive segregation at regions close to the cooled surface of the casting with an Al-6wt.%Mg alloy. They attributed this behavior to the effect of solidification shrinkage followed by interdendritic flow of the Mg-enriched melt. In the present study, it seems that an equilibrium has been established between upward gravity-driven Mg and downward shrinkage effects. Fe is normally a residual element of commercially pure Al. An average content of 0.15wt%Fe was observed along the entire DS casting length. A higher Fe content at the region immediately ahead the cooled bottom of the casting is shown in Figure 2(b). This enrichment of Fe is caused by Fe diffusion from the steel sheet that separates the casting from the cooling water [18].

The cooling curves during solidification, shown in Figure 3(a), were obtained from a set of thermocouples placed in the geometrical center of the cylindrical mold cavity along its length. Figure 3(b) shows the plot of position (P) from the metal/mold interface and the corresponding time (t) of the liquidus front passing by each thermocouple. A $P(t)=a.t^b$ type function was fitted to the experimental data, being "a" and "b" constants. The derivatives of these functions with respect to time gave values for the growth rate (V_L), as shown in Figure 3(c). The cooling rate ($\dot{T}$) was determined along the castings lengths, by considering the derivatives with respect to time of the thermal data recorded immediately after the passage of the liquidus front by each thermocouple. The resulting experimental $\dot{T}$ profile is shown in Figure 3(d).

(a)   (b)
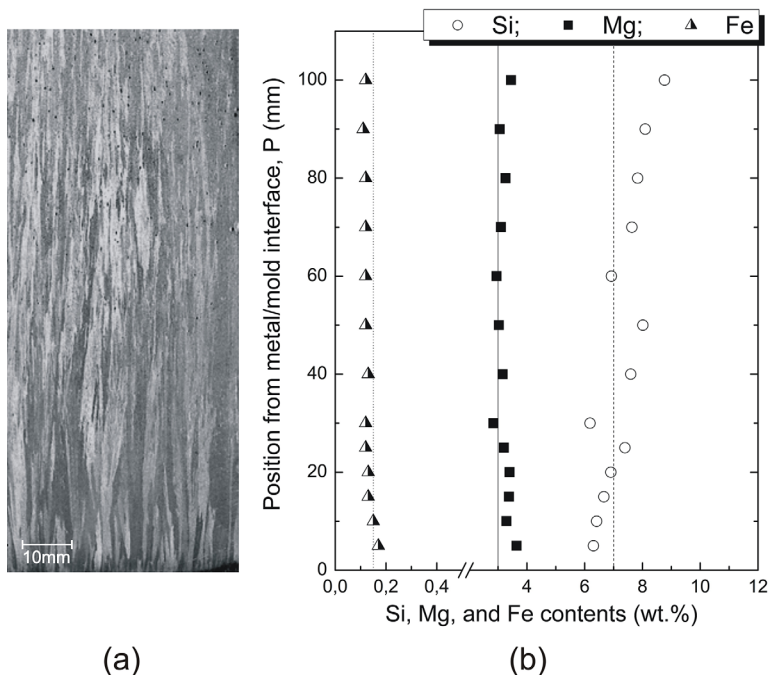
Figure 2. a) Macrostructure of Al-7wt.%Si-3wt.%Mg alloy DS casting; **b)** Macrosegregation profiles for silicon, magnesium and iron along the DS casting length.

Dendritic Spacing and Macrosegregation Affecting Microhardness of an Al-Si-Mg Alloy Solidified Under
Unsteady State Conditions

5

Figure 3. a) Experimental cooling curves for different positions along the length of the DS Al-7wt.%Si-3wt.% alloy casting; **b)** Position from the metal/mold interface as a function of time; **(c)** Growth rate; and **(d)** cooling rate as a function of position from the metal/mold interface.

Figure 4 shows microstructures obtained by optical microscopy from cross and longitudinal sections of the DS casting. Three representative samples exhibit a typical microstructure morphology composed by an Al-rich dendritic matrix [17,23,26,27]. There are two types of eutectic mixtures in the interdendritic regions: 1) ternary eutectic: Al + Si particles + Mg_2Si + Fe-rich IMC and 2) binary eutectic: Al + Mg_2Si, as will be shown further. Close to the metal/mold interface, a mo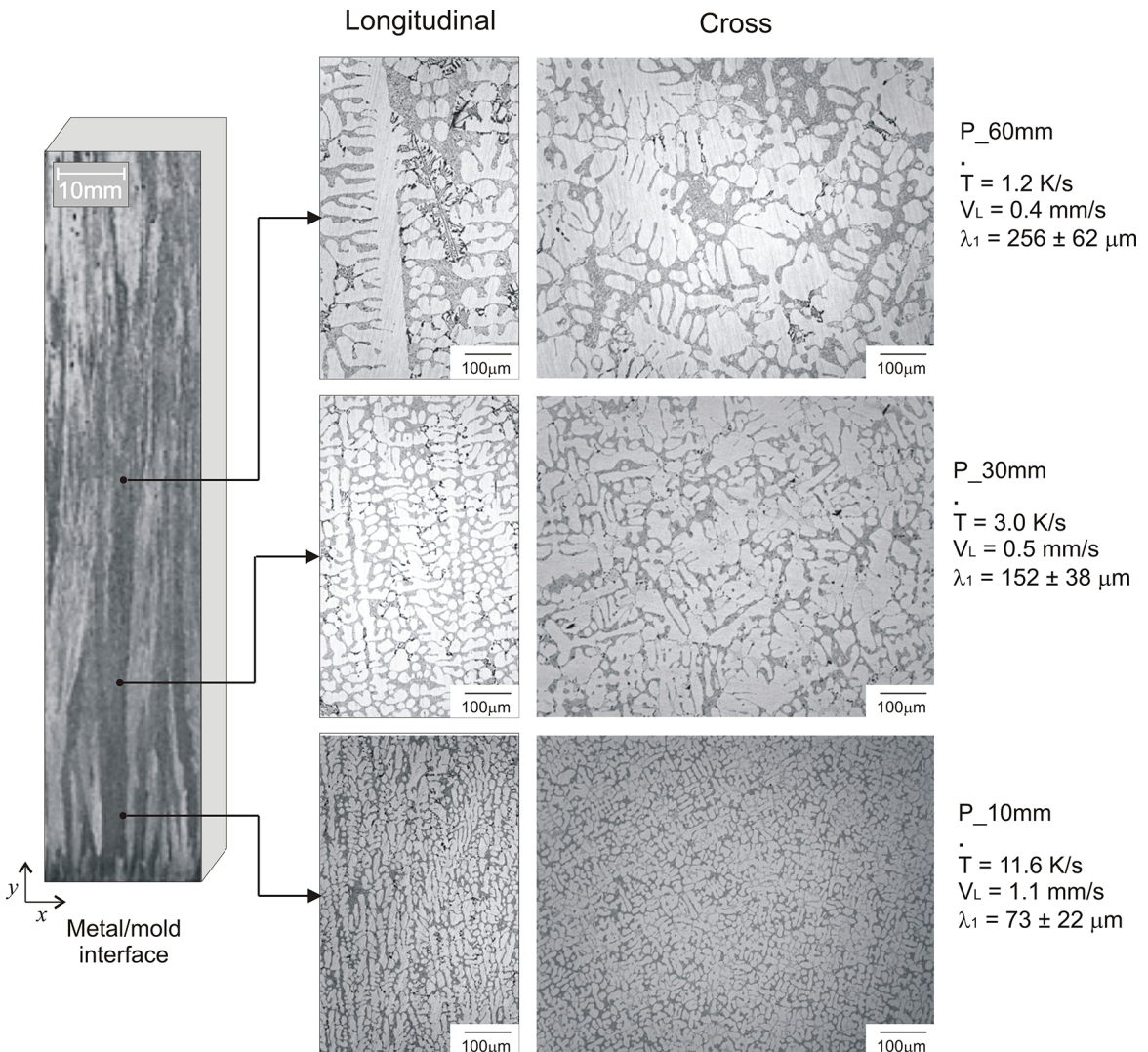re refined morphology can be observed due to the highest values of growth rates and cooling rates in this region. On the other hand, with the increase in distance from the cooled bottom of the casting, V_L and $\dot{T}$ progressively decrease and the dendrite coarsening progresses. The results obtained in this research showed the beginning of the growth of tertiary dendritic arms (λ_3) for cooling rates lower than 6K/s, which stabilizes for cooling rates lower than 3K/s. It is possible to verify the regular presence of this type of dendritic arm in Figure 4, sample P_30mm (longitudinal view). Rosa et al. [27]

analyzed the tertiary dendritic growth of binary hypoeutectic Al-Si alloys solidified in unsteady state conditions. The authors reported that a composition of 7wt% Si only showed stable λ_3 growth conditions to for cooling rates lower than 2K/s. The addition of 3wt% Mg seems to have anticipated the destabilization of the solid/liquid interface at the secondary dendritic arms favoring the growth of tertiary dendritic arms for higher values of cooling rate.
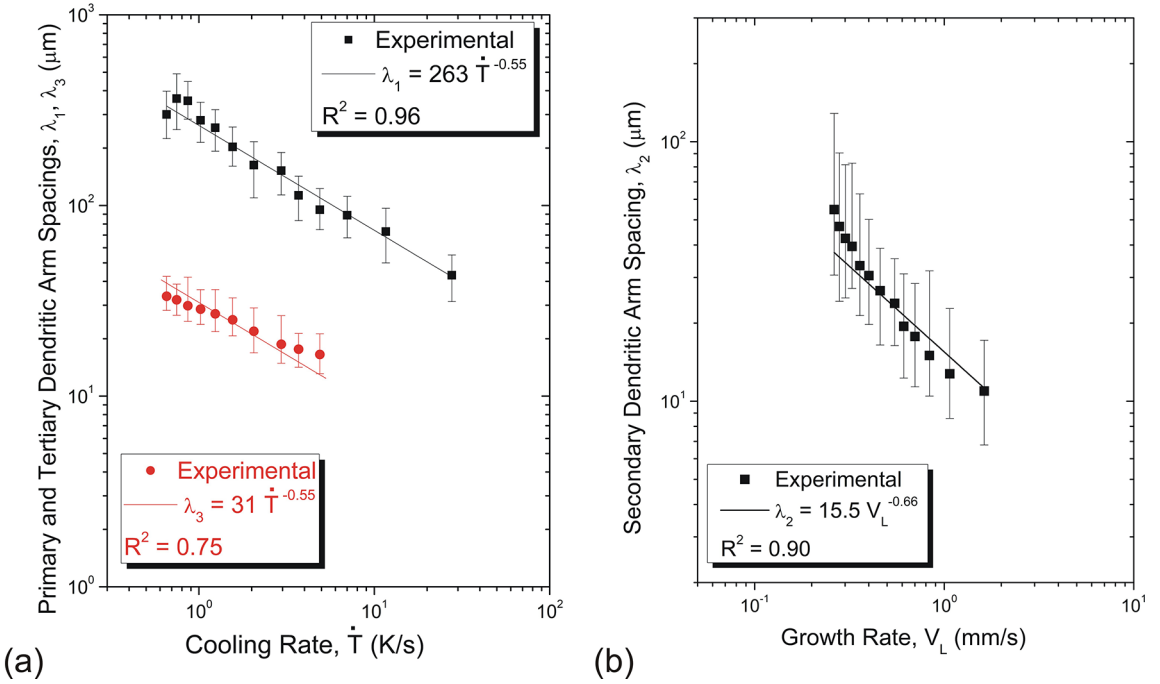
Figure 5 shows the evolution of the microstructural parameters λ_1, λ_2 and λ_3 as a function of the solidification thermal parameters V_L and $\dot{T}$. In the development of experimental power functions relating the growth of λ_1 in unsteady state conditions as a function of $\dot{T}$, several authors [17,18,23,26,27] have derived a same exponent: -0.55. In the present study λ_1 has been correlated with $\dot{T}$ by a power function given by $\lambda_1 = 263 \ \dot{T}^{-0.55}$, as shown in Figure 5a. Peres et al. [16] obtained an experimental growth law of λ_1 as a function of $\dot{T}$ given by $\lambda_1 = 220 \ \dot{T}^{-0.55}$, for hypoeutectic Al-Si alloys. Comparing the growth of λ_1 for the DS Al-7wt%Si-3wt%Mg

casting with that of an Al-7wt% Si [17] alloy, it was observed that the addition of 3wt.% Mg induced an increase in λ_1 for a same cooling rate range.

The experimental correlation λ_2 vs $\dot{T}$ for the DS Al-7wt%Si-3wt%Mg alloy casting, shown in Figure 5(b), is given by . For the Al-7wt.%Si [16] the literature reports . By comparing the aforementioned λ_2 growth laws, it can be seen that the addition of Mg to the Al-7wt.%Si alloy resulted on an opposite effect as compared to that associated with λ_1, i.e. λ_2 decreases with the addition of Mg. In this work, the tertiary dendritic arms, λ_3, were identified and measured accordingly, as depicted in Figure 5(a). The same exponent used for primary dendritic growth (-0.55) can represent the evolution of λ_3 with $\dot{T}$, $\lambda_3 = 31 \ \dot{T}^{-0.55}$. The average λ_3 values varied from 16.5 to 34.4 μm. Rosa et al. [26] evaluated the value of λ_3 for hypoeutectic Al-Si alloys and proposed the following experimental growth law $\lambda_3 = 18 \ \dot{T}^{-0.55}$. In this case, the addition of Mg (similarly to the growth of λ_1) increases λ_3 for a same $\dot{T}$, as compared to results of binary hypoeutectic Al-Si alloys.

Longitudinal   Cross

P_60mm
$\dot{T}$ = 1.2 K/s
V_L = 0.4 mm/s
λ_1 = 256 ± 62 μm

10mm

P_30mm
$\dot{T}$ = 3.0 K/s
V_L = 0.5 mm/s
λ_1 = 152 ± 38 μm

P_10mm
$\dot{T}$ = 11.6 K/s
V_L = 1.1 mm/s
λ_1 = 73 ± 22 μm

y
x
Metal/mold interface

100μm

Figure 4. Typical optical microstructures of longitudinal (left) and cross (right) sections of the DS Al-7wt.%Si-3wt.%Mg alloy casting.

Dendritic Spacing and Macrosegregation Affecting Microhardness of an Al-Si-Mg Alloy Solidified Under
Unsteady State Conditions

7

Figure 5. Correlations between dendrite arm spacings and solidification thermal parameters: **a)** λ_1 and λ_3 evolution as a function of cooling rate; and b) λ_2 evolution as a function of growth rate for the ternary Al-7wt.%Si-3wt.%Mg alloy casting.

Secondary phases or intermetallic compounds (IMCs) were characterized by X-ray Diffraction and Scanning Electron Microscope (SEM) equipped with an Energy Dispersive Spectrometer (EDS). As shown in Figure 2(b) the Al-7wt. Si-3wt.%Mg alloy has a residual content of Fe of about 0.15wt.%. This content is enough to change the equilibrium pseudo-binary-phase diagram shown in Figure 1(a). Therefore, a Scheil-Gulliver (S-G) simulation was carried out in order to predict the new phases due to this residual Fe content. According to S-G computations performed by the Thermo-Calc Software, 0.15wt.%Fe enabled partial precipitations to occur during solidification, as shown in Figure 6(a). This is in agreement with the observations reported by Lima et al.[27] who identified on an Al-7wt.Si-0.3wt.%Mg alloy, the growth of α-Al, Si, Mg_2Si, β-AlSiFe and π-AlSiMgFe. Figure 6(b) shows the XRD analysis that identified the following phases: α-Al, Si, Mg_2Si and π-AlSiMgFe. Essentially, these are the same IMCs which were predicted by the Scheil-Gulliver computations.
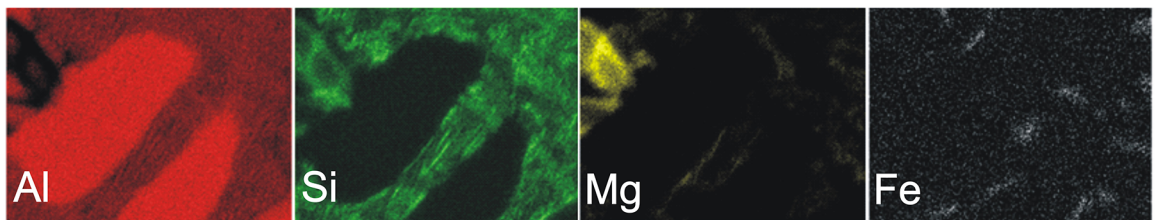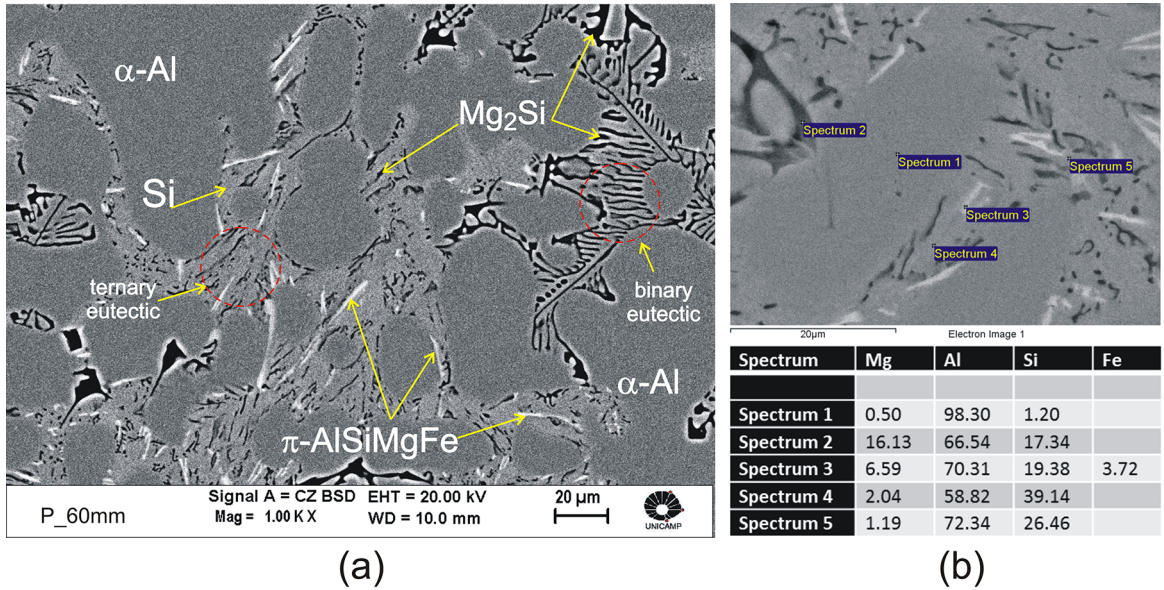
The addition of 3wt.%Mg to the Al-7wt%Si alloy produced a more complex microstructure, with the formation of larger fraction of secondary phases. Figure 7(a) shows the morphology of the secondary phases for a cooling rate of 1.2K/s. In the region of binary eutectic, the morphology of the Mg_2Si phase is a Chinese-script like [28]. This IMC occurred for the entire range of analyzed cooling rates, as part of the eutectic binary with Al, or still combined with Si and Fe-rich phase at the ternary eutectic mixture. The morphology of the Fe-rich phase was strongly influenced by the reduction

in the cooling rate. For $\dot{T} > 3K/s$ these phases formed more frequently in the form of tertiary eutectic. For $\dot{T}$ lower than 1K/s, the tendency is to generate an acicular morphology. The composition of each phase was presented in a table inside Figure 7(b). Figure 7(c) shows SEM/EDS analyses with EDS elemental mapping indicating the composition and distribution of the elements in each phase. Liu and Kang [27] reported that the addition of Mg to Al-Mg-Si alloys has a strong influence on the formation of the solidification microstructures. The increase in the Mg content favors the increase in the fraction of Mg_2Si particles. These authors also observed that the presence of Fe segregation to the final zone of solidification lead to the formation of a complex IMC (Al, Fe, Mg, Si), as well as of a tertiary eutectics, evidencing that even low Fe contents should not be neglected.

Figure 8(a) shows a plot of the Mg content[19] in solid solution (Mg_{SS}) in the Al-rich matrix along the length of the DS Al-7wt.%Si-3wt.%Mg alloy casting, determined by SEM/EDS for three samples. A reduction in Mg_{SS} can be observed from bottom to top of the casting thus allowing a higher content of free Mg (Mg_F) to be available, with the other alloy elements, to form the IMCs. Mg has a relatively high solubility in Al [29]. However, as the temperature is reduced a decrease in solubility occurs, and at room temperature Mg has a maximum solubility of approximately 0.4wt.%. In Al-Si-Mg alloys, Mg_2Si formation occurs when Mg and Si are present at a Mg/Si ratio of 1.73, and its fraction will be proportional to the Mg content in the alloy [30]. According to Closset and Gruzleski [31], the formation of iron-rich IMC is influenced by the Mg content. With more
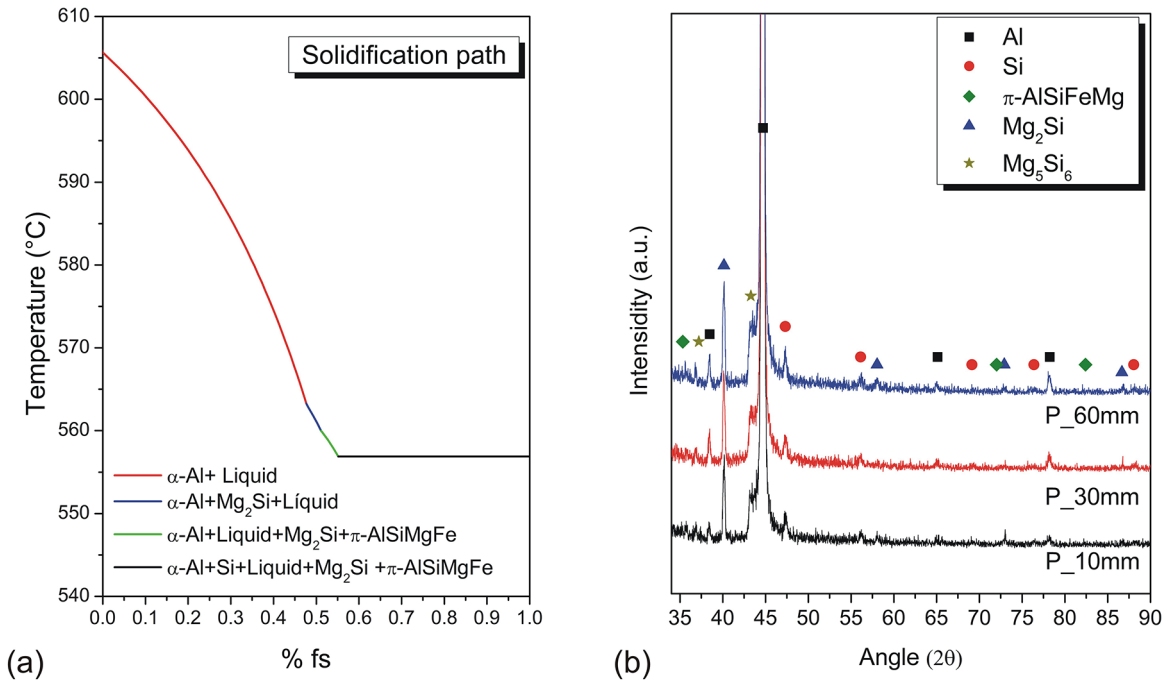
Figure 6. a) Scheil-Gulliver simulation calculated by the Thermo-Calc software with addition of 0.15wt.%Fe; **b)** X-ray diffraction (XRD) patterns for three different positions (P) and cooling rates along the DS casting length.


Spectrum	Mg	Al	Si	Fe
Spectrum 1	0.50	98.30	1.20	
Spectrum 2	16.13	66.54	17.34	
Spectrum 3	6.59	70.31	19.38	3.72
Spectrum 4	2.04	58.82	39.14	
Spectrum 5	1.19	72.34	26.46	

Figure 7. (a) SEM micrograph; **(b)** SEM/EDS microprobe analyses points 1-5 indicate local wt.% concentration of Al/Si/Mg/Fe; and **(c)** elemental SEM/EDS mapping.

Dendritic Spacing and Macrosegregation Affecting Microhardness of an Al-Si-Mg Alloy Solidified Under
Unsteady State Conditions

9

Mg_F at positions far from the cooled bottom of the casting, the volume fractions of Mg_2Si and π-AlSiMgFe IMCs increase, as can be observed in Figure 8 (b). In order to confirm this reasoning, image analyses using the Image-J software were carried out. The mean values of area fractions and shape factors of the Mg_2Si (dark particles) and π-AlSiMgFe IMCs (white particles) in the SEM images of Figure 7 have been determined for any cooling condition analyzed. In Figure 8(b)

it can be observed a reduction in circularity of both IMCs with decreasing cooling rates (middle gray column). A reverse tendency can be observed for the fraction and aspect ratio, which increased with slower cooling conditions. Mg_2Si and π-AlSiMgFe IMCs showed quite close values of circularity and aspect ratio along the entire length of the DS casting. The π-AlSiMgFe IMC shows higher aspect ratios associated with the decrease in cooling rate.
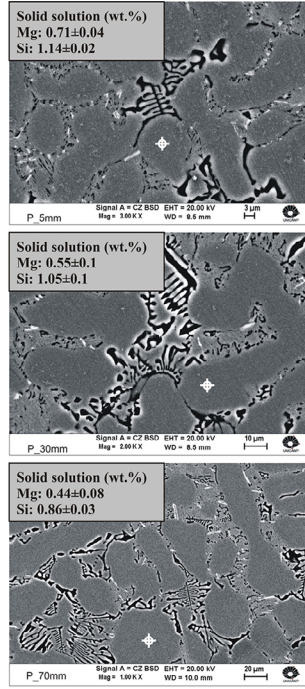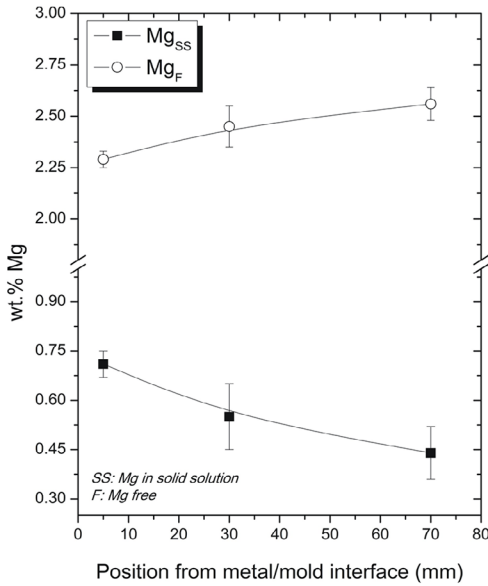

(a)
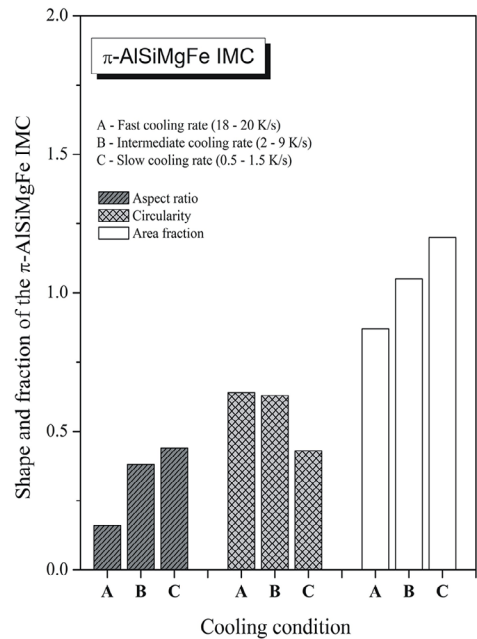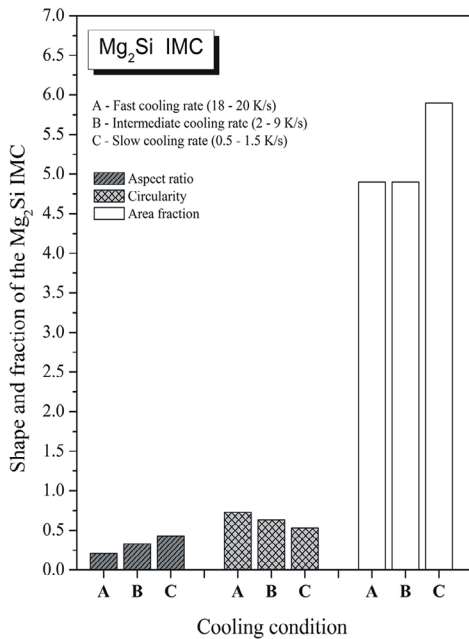
(b)

Figure 8. a) Mg solid solution content in α-Al matrix, and **b)** Column graphs of average IMCs particles aspect ratio, circularity and area fraction for different ranges of solidification cooling rates along the length of the DS Al–7wt.% Si–3wt.%Mg alloy casting.

The higher fraction of Mg_2Si IMC is related to the local contents of Mg and Si, since in Al-Si-Mg alloys the Mg_2Si fraction is proportional to both Mg and Si contents of the alloy. It is worth noting that for positions in the casting associated with lower cooling rates a higher amount of Si is available due to macrosegregation effects (Figure 2), which combined with the higher Mg_F amount (Figure8a) favors the formation of higher fractions of both IMCs.

Vickers microhardness tests were performed in transverse samples extracted along the entire DS casting length. Figure 9 shows the experimental measured values of Vickers microhardness as a function of the square root of λ_2. Two different trends on the evolution of HV with $\lambda_2^{-1/2}$ can be observed (characterized by an inflection point at $\lambda_2^{-1/2} = 0.19 \mu m^{-1/2}$). The adoption of two Hall-Petch type relationships seems to be appropriate for representing the hardness evolution with λ_2 for the examined alloy. Figure 4 showed stable growth of λ_3 from a lower cooling rate 3K/s. Despite the relatively small variation of λ_2 and λ_3 values along the monitored levels of cooling rates, other metallurgical features may interfere on hardness. In recent work, Kim et al. [32], using compression and nanoindentation

tests, have evaluated the deformation mechanism of an Al-Cu-Si alloy. A fractographic analysis carried out by using atomic force microscopy (AFM) showed that the enhancement of mechanical properties was due to the combined contributions of shear banding mechanisms associated with cooperative boundary sliding/rotation. Additionally, nanoindentation analyses confirmed that the interfacial sliding occurred during plastic deformation at the dendrite (soft)/eutectic (hard) interface.

Regions having higher values of λ_1 along the length of a DS casting are associated with higher values of λ_2 and λ_3, which are generally associated with smaller values of hardness as compared to regions of smaller dendritic spacings [11]. As shown in Figure 9, this is so for the HV profile from the lowest λ_2 experimental value (highest $\lambda_2^{-1/2}$ value) up to the inflection point [11,18], from which HV increases with decreasing dendritic spacings, that is for cooling rates lower than 2K/s, HV increases with the increase in λ_1, λ_2 and λ_3 (decrease in $\lambda_2^{-1/2}$). Such increase in hardness even with increasing dendritic spacings can be attributed to the plastic constraint promoted by increasing fractions of hard π-AlSiFeMg and Mg_2Si IMCs in regions closer to the top of the DS casting.
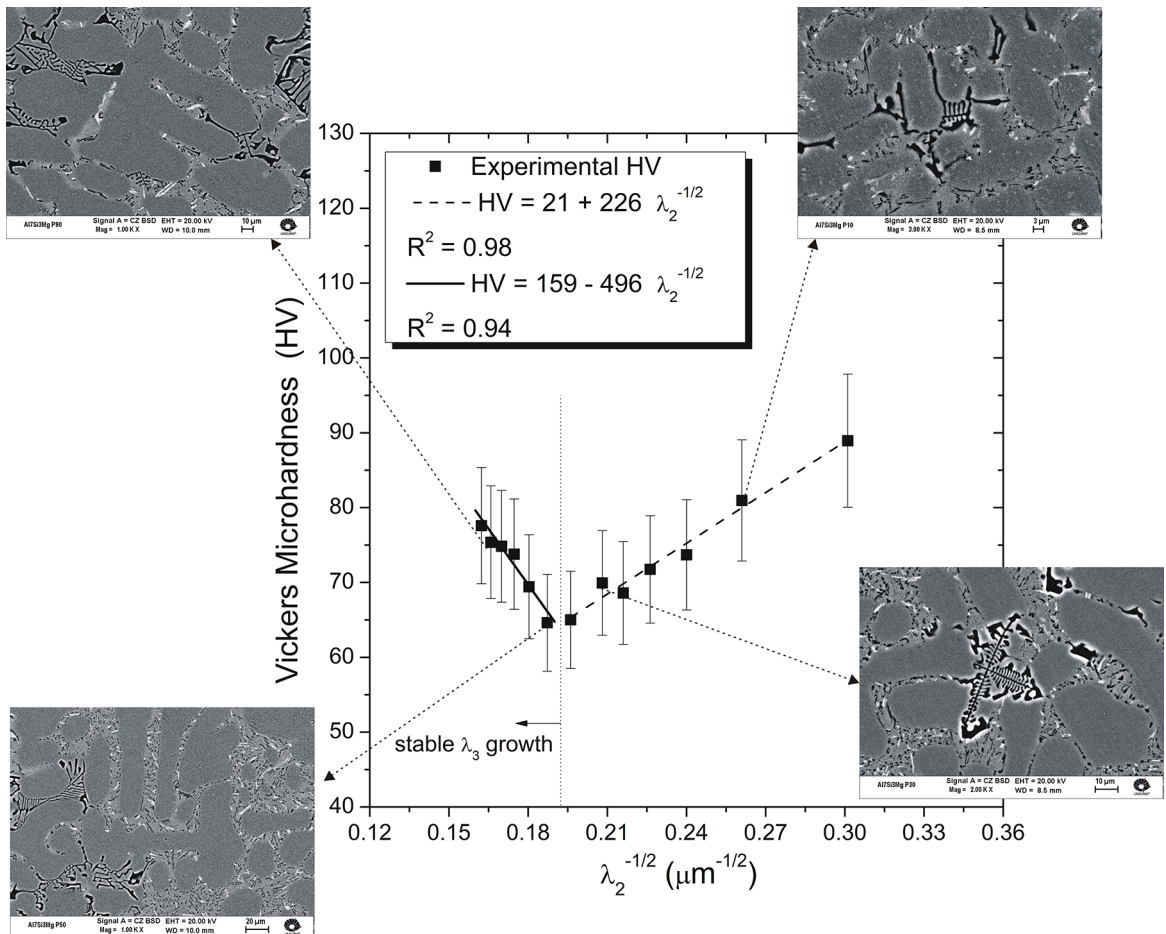
Figure 9. Evolution of Vickers Microhardness with the square root of secondary dendritic arm spacing.

Dendritic Spacing and Macrosegregation Affecting Microhardness of an Al-Si-Mg Alloy Solidified Under
Unsteady State Conditions

11

4. Conclusions

The following conclusions can be drawn from the present experimental study:

A Si macrosegregation profile ranging from 6wt.% to 8.5wt.% at the bottom and top of the DS casting, respectively, was observed. No macrosegregation of Mg was observed along the entire casting, despite the occurrence of Mg-enriched liquid (less dense than the global melt). It seems that a balance occurred between upward gravity-driven and downward shrinkage flow contributions, thus leading to a resultant stable concentration profile.

A dendritic morphology was shown to characterize the Al-rich matrix along the DS casting. Within the interdendritic regions two types of eutectic mixtures could be observed: 1) ternary eutectic: $Al + Si$ particles $+ Mg_2Si + Fe$-rich IMC and 2) binary eutectic: $Al + Mg_2Si$.

Experimental growth laws were proposed correlating the dendritic spacings (λ_1, λ_2, and λ_3) to the thermal solidification parameters (V_L and $\dot{T}$). These experimental laws are the only approaches permitting the design of the scale of the dendritic pattern of such alloy as a function of unsteady-state solidification thermal parameters.

The dependence of Vickers microhardness on λ_2 were experimentally established by Hall–Petch type relationships. It was shown that HV increases with decreasing dendritic spacings up to an inflection point associated with a solidification cooling rate of 2K/s. For cooling rates < 2K/s, HV increases with further increase in dendritic spacings, and such increase in hardness was attributed to the increasing fractions of hard π-AlSiFeMg and Mg_2Si IMCs at regions close to the top of the casting, which were formed due to both Si macrosegregation and higher content of free Mg.

5. Acknowledgements

6. References

1. Javidani M, Larouche D. Application of cast Al–Si alloys in internal combustion engine components. *International Materials Reviews*. 2014;59(3):132-58.

2. Ye H. An overview of the development of Al-Si-alloy based material for engine applications. *Journal of Materials Engineering and Performance*. 2003;12(3):288-97.

3. Timelli G, Caliari D, Rakhmonov J. Influence of process parameters and Sr addition on the microstructure and casting defects of LPDC A356 alloy for engine blocks. *Journal of Materials Science and Technology*. 2016;32(6):515-23.

4. Tebib M, Samuel AM, Ajersch F, Chen XG. Effect of P and Sr additions on the microstructure of hypereutectic Al–15Si–14Mg–4Cu alloy. *Materials Characterization*. 2014;89:112-23.

5. Kashyap KT, Murali S, Raman KS, Murthy KSS. Casting and heat treatment variables of AI-7Si-Mg. *Materials Science and Technology*. 1993;9(3):189-204.

6. Glazoff M, Khvan A, Zolotorevskiy VS, Belov NA, Dinsdale A. *Casting aluminum alloys*. Amsterdam: Butterworth-Heinemann; 2007.

7. Bray JW. Aluminum mill and engineered wrought products. In: *Properties and selection: nonferrous alloys and special-purpose materials*. Materials Park, OH: ASM International; 1990. v. 2. p. 29-61.

8. Mandal A, Makhlouf MM. Chemical modification of morphology of Mg_2Si phase in hypereutectic aluminium–silicon–magnesium alloys. *International Journal of Cast Metals Research*. 2010;23(5):303-9.

9. Rana RS, Purohit R, Das S. Reviews on the influences of alloying elements on the microstructure and mechanical properties of aluminum alloys and aluminum alloy composites. *International Journal of Scientific and Research Publications*. 2012;2(6):1-7.

10. Li Q, Li B, Li J, Xia T, Lan Y, Guo T. Effects of the addition of Mg on the microstructure and mechanical properties of hypoeutectic Al–7%Si alloy. *International Journal of Metal Casting*. 2017;11(4):823-30.

11. Bertelli F, Brito C, Ferreira IL, Reinhart G, Nguyen-Thi H, Mangelinck-Noël N, et al. Cooling thermal parameters, microstructure, segregation and hardness in directionally solidified Al–Sn-(Si;Cu) alloys. *Materials and Design*. 2015;72:31-42.

12. Kim JT, Hong SH, Park JM, Eckert J, Kim KB. Microstructure and mechanical properties of hierarchical multi-phase composites based on Al-Ni-type intermetallic compounds in the Al-Ni-Cu-Si alloy system. *Journal of Alloys and Compounds*. 2018;749:205-10.

13. Wu X, Zhang H, Zhang F, Ma Z, Jia L, Yang B, et al. Effect of cooling rate and Co content on the formation of Fe-rich intermetallics in hypoeutectic Al7Si0.3Mg alloy with 0.5%Fe. *Materials Characterization*. 2018;139:116-24.

14. Canté MV, Lima TS, Brito C, Garcia A, Cheung N, Spinelli JE. An alternative to the recycling of Fe-contaminated Al. *Journal of Sustainable Metallurgy*. 2018;4(3):412-26.

15. Kumar S, Grant PS, O'Reilly KAQ. Fe bearing intermetallic phase formation in a wrought Al-Mg-Si alloy. *Transactions of the Indian Institute of Metals*. 2012;65(6):553-7.

16. Taylor JA. *The effect of iron in Al-Si casting alloys*. In: 35th Australian foundry institute national conference; 2004 oct 31-nov 3; Adelaide, South Australia. Adelaide: Australian Foundry Institute (AFI); 2004. p. 148-157.

17. Peres MD, Siqueira CA, Garcia A. Macrostructural and microstructural development in Al–Si alloys directionally solidified under unsteady-state conditions. *Journal of Alloys and Compounds*. 2004;381(1-2):168-81.

18. Brito C, Reinhart G, Nguyen-Thi H, Mangelinck-Noël N, Cheung N, Spinelli JE, et al. High cooling rate cells, dendrites, microstructural spacings and microhardness in a directionally solidified Al-Mg-Si alloy. *Journal of Alloys and Compounds*. 2015;636:145-9.

19. Brito C, Vida T, Freitas E, Cheung N, Spinelli JE, Garcia A. Cellular/dendritic arrays and intermetallic phases affecting corrosion and mechanical resistances of an Al–Mg–Si alloy. *Journal of Alloys and Compounds*. 2016;673:220-30.

20. Vida TA, Feitosa ESF, Brito C, Cheung N, Arenas MA, Conde A, et al. Thermal parameters and microstructural development in directionally solidified Zn-Rich Zn-Mg alloys. *Metallurgical and Materials Transactions: A*. 2016;47(6):3052-64.

21. Gündüz M, Çadırlı E. Directional solidification of aluminium-copper alloys. *Materials Science and Engineering: A*. 2002;327(2):167-85.

22. American Society for Testing and Materials (ASTM). *E384-17 – Standard test method for microindentation hardness of materials*. West Conshohocken, PA: ASTM International; 2017. p. 1-40.

23. Gomes LG, Moutinho DJ, Ferreira IL, Rocha OL, Garcia A. The growth of secondary dendritic arms in directionally solidified Al-Si-Cu alloys: a comparative study with binary Al-Si alloys. *Applied Mechanics and Materials*. 2015;719-720:102-5.

24. Committee – American Institute of Hydrology (AIH). *Metals handbook: properties and selection–nonferrous alloys and pure metals*. Russel Township, OH: ASM Handbook; 1990. v. 2.

25. Vreeman CJ, Incropera FP. The effect of free-floating dendrites and convection on macrosegregation in direct chill cast aluminum alloys: Part II: predictions for Al–Cu and Al–Mg alloys. *International Journal of Heat and Mass Transfer*. 2000;43(5):687-704.

26. Rosa DM, Spinelli JE, Garcia A. Tertiary dendrite arm spacing during downward transient solidification of Al–Cu and Al–Si alloys. *Materials Letters*. 2006;60(15):1871-4.

27. Lima JO, Barbosa CR, Magno IAB, Nascimento JM, Barros AS, Oliveira MC, et al. Microstructural evolution during unsteady-state horizontal solidification of Al-Si-Mg (356) alloy. *Transactions of Nonferrous Metals Society of China*. 2018;28(6):1073-83.

28. Liu YL, Kang SB. The solidification process of Al – Mg – Si alloys. *Journal of Materials Science.* 1997;2(32):1443-7.

29. Massalski TB, Murray JL, Bennett LH, Baker H. *Binary alloy phase diagrams.* Metals Park, OH: American Society for Metals; 1986. v. 1-2.

30. Caceres CH, Davidson CJ, Griffiths JR, Wang QG. The effect of Mg on the microstructure and mechanical behavior of Al-Si-Mg casting alloys. *Metallurgical and Materials Transactions: A*. 1999;30(10):2611-8.

31. Closset B, Gruzleski JE. Structure and properties of hypoeutectic Al-Si-Mg alloys modified with pure strontium. *Metallurgical Transactions: A*. 1982;13(6):945-51.

32. Kim JT, Hong SH, Kim YS, Park HJ, Maity T, Chawake N, et al. Cooperative deformation behavior between the shear band and boundary sliding of an Al-based nanostructure-dendrite composite. *Materials Science and Engineering: A*. 2018;735:81-8.